ACS OMEGA

Open Access

http://pubs.acs.org/journal/acsodf

Article

Velocity and Temperature Simulation for a Cylindrical Regenerative Thermal Oxidizer

Kaiming Ren, Zhijun Zhang, Haixiang Qin, Jianyu Tan, and Xiaowen Hao*

Cite This: *ACS Omega* 2024, 9, 15893−15903

Read Online

ACCESS | Metrics & More | Article Recommendations

ABSTRACT: The cylindrical regenerative thermal oxidizer (CRTO) came into being later than the three-chamber regenerative thermal oxidizer (TRTO). Compared with TRTO, CRTO has a smaller size and a larger regenerator volume for absorbing and releasing heat. There are few studies on CRTO despite its numerous applications. A CRTO was selected in industrial applications for simulation research. The velocity and temperature of the CRTO were investigated after error analysis of industrial and simulated data. It was found that the velocity and temperature in the regenerative chamber had obvious stratification and gradients after homogenization by the regenerator unit. The velocity and temperature distribution in the oxidation chamber were independent of the position of the CRTO inlet and outlet or the structure below the regenerator, and there were identical periodic changes in each period. A TRTO with primary parameters as those of the CRTO was employed for comparison. The time of the intake and exhaust periods of a CRTO regenerative chamber were 30 s longer than those of a TRTO. The regenerator volume of heat storage used by CRTO for heat exchange increased by 1/6 compared to that of TRTO at the same total regenerator volume. Simulation shows that CRTO had a more uniform velocity and temperature in the regenerative chamber compared to those in TRTO, increasing by approximately 2%; the thermal efficiency is higher, with an average increase of about 3%.

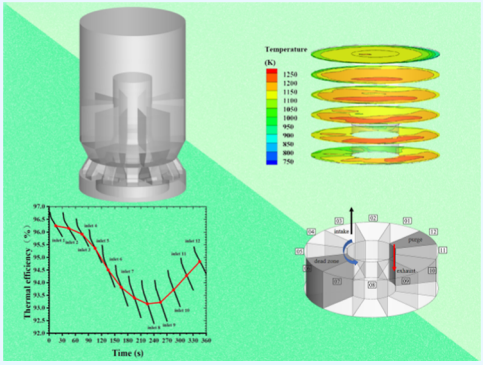

1. INTRODUCTION

Introduced into the industry by Hamon Research Cottrell Company,[1] the regenerative thermal oxidizer (RTO) technology has been used to treat volatile organic compounds (VOCs) in environmental protection.[2] The regenerator made of ceramics is applied in the regenerative chamber of the RTO. The regenerator stores or releases much of VOCs' combustion heat with high thermal efficiency.[3,4] RTO can operate without an external fuel at low VOC concentrations due to the sufficient energy provided by the regenerator.[5−7] Therefore, energy saving could be accomplished.[8,9] In addition, RTO is suitable for treating almost all types of VOCs.

RTO mainly consists of an oxidation chamber and multiple regenerative chambers. During RTO operation, the intake gas with VOCs and the purge airflow flowed upward into the regenerative chambers, respectively. They absorb heat from the regeneration chamber and then flow into the oxidation chamber.[10] These two processes are referred to as the intake period and the purge period, respectively. The VOCs are oxidized in the oxidation chamber. The high-temperature exhaust gas flows downward from the oxidation chamber to the regenerative chamber and releases heat, which is called the exhaust period. For the cuboid-shaped RTO, the three periods above form a cycle. The intake and exhaust periods occupy an equal number of the regenerative chambers, while purging occupies only one. Therefore, the cuboid-shaped RTO has an odd number of regenerative chambers, which is divided into 3 chambers (corresponding to the three-chamber RTO, TRTO), 5 chambers, and 9 chambers. Cylindrical RTO (CRTO) adds a regenerative chamber without gas flow, termed the dead zone, between the intake and exhaust regenerative chambers. Its purpose is to prevent the intake gas from bypassing the regenerative chambers and proceeding directly to the RTO outlet. The number of common CRTO regenerative chambers is 12.[11]

Many research studies have been conducted on the cuboid-shaped RTO, focusing on the regenerative chamber and the regenerative chamber channel.[12−15] The research included the influence of operating parameters on the temperature and heat transfer in the regenerative chamber, such as structural parameters of the regenerator and regenerative chamber,[16−19] switching time,[20−23] and superficial velocity.[17,21,22,24] Due to the homogenization effect by the regenerator unit, the gas flow exhibited a relatively uniform velocity and temperature

Received: October 23, 2023
Revised: March 1, 2024
Accepted: March 7, 2024
Published: March 26, 2024

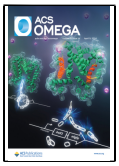

(a) External structure (b) Lower part

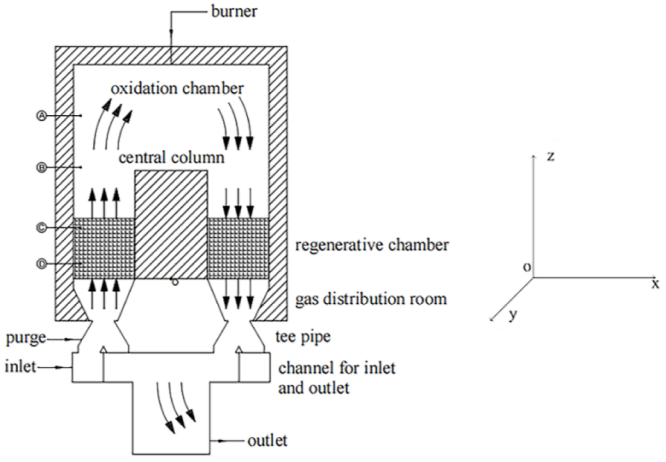

(c) Internal structure

Figure 1. Industrial CRTO external (a,b) and internal structures (c).

distribution in the cross-section perpendicular to the flow direction. Researchers presented different findings. Hao[21] found that the side length of the regenerator was the most important factor for thermal efficiency and heat transfer coefficient. The switching time and channel thickness had little impact on the thermal efficiency. The superficial velocity and channel thickness of the regenerator had little effect on the heat transfer coefficient. Along the flow direction, the velocity, temperature, and heat transfer all showed periodic changes.[25] Hao[26] studied the uniformity of the velocity and temperature in the regenerative chamber: the two parameters showed high uniformity after the gas flowed through the honeycomb regenerator.

The research on the regenerative chamber was also extended to the entire cuboid-shaped RTO. Although its average thermal efficiency could reach 90%,[27−29] the residence time in each period within the oxidation chamber varied greatly, resulting in a nonuniform distribution of velocity and temperature within the oxidation chamber.[19,30] This was due to the odd number of regenerative chambers and cuboid-shaped oxidation chamber. The different intake and exhaust regenerative chambers at different periods resulted in differences in the gas flow paths.

The advantages of CRTO are its smaller size and compact structure. The regenerative chamber of the CRTO in the purge period is 1/12 of the total regenerative chambers, while the TRTO in the cuboid-shaped RTO is 1/3. The purge airflow flows with normal temperature but without VOCs. It blows the VOCs remaining in the regenerative chamber into the oxidation chamber for decomposition, thereby improving the removal efficiency of VOCs. However, a purge occupying too much regenerator volume will reduce the heat exchange volume, thereby diminishing thermal efficiency.

As one of the core components of CRTO, the switching valves guide the gas flow in and out. There are two types of switching valves under the CRTO regenerator. One is the rotary valve driven by a reducer. Valves of the second type are similar to the cuboid-shaped RTO. That is, each regenerative chamber corresponds to three valves, namely, the intake, exhaust, and purge valves. There are 36 valves in the 12 regenerative chambers. The second type was selected.

There have been few studies about CRTO in China despite its wide application. Similar cylindrical heat exchange structures were mainly rotary air preheaters and gas−gas heat exchangers (GGHs).[31−33] The velocity and temperature in the heat exchanger were relatively uniform, and periodic

https://doi.org/10.1021/acsomega.3c08352
ACS Omega 2024, 9, 15893−15903

modifications would occur due to rotation. Mao[34] found that the temperature was quite stable with time in the regenerator of a rotary flow reversal reactor.

Due to its high thermal efficiency and VOCs' emissions meeting Chinese standards, more than 500 units of RTO were applied in 2016 alone.[35] In recent years, some Chinese environmental protection companies have made hundreds of industrial applications. Moreover, competition among RTOs is becoming increasingly fierce, resulting in low quotations. Installing more regenerators can improve the thermal efficiency, and increasing the temperature of the oxidation chamber can meet the emission standards. But these methods will increase the investment or operational costs. Meanwhile, RTO has a large number of regenerator volumes with a large amount of heat storage, resulting in a slow response to parameter adjustments. In addition, the local emission standard for VOCs in some areas of China has shifted from 50 to 30 mg/m^3.[36] Further studies are needed if the RTO intends to satisfy low-price and high-efficiency requirements.

This research was based on a CRTO application, whose inlet gas flux was 10,000 m^3/h. After verification with industrial data, the distribution of longitudinal velocity and temperature within the CRTO in a cycle was studied. A comparison was made with a TRTO in a cycle regarding the average velocity and temperature in the regenerative chamber. A comparative analysis was conducted to assess the homogeneity of the velocity and temperature. Finally, the thermal efficiency was analyzed between the CRTO and TRTO.

2. INTRODUCTION OF THE MODEL AND METHODS

2.1. Model Introduction. Figure 1 shows the industrial CRTO's external and internal structures. It mainly consists of the channel for the inlet and outlet, the tee pipe, the gas distribution room, the regenerative chamber, and the oxidation chamber. The intake enters the gas distribution room from the tee pipe. Then, it flows through five adjacent fan-shaped regenerative chambers (inlet chambers) (Figure 2) to absorb

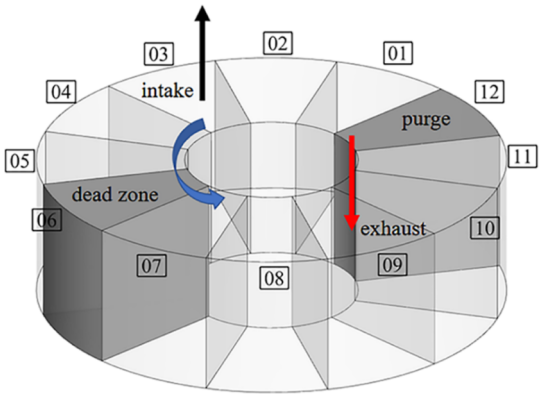

Figure 2. Regenerative chamber number and chamber status.

the heat of the regenerators before flowing into the oxidation chamber. VOCs are burned in the oxidation chamber. After combustion, the high-temperature exhaust enters five adjacent regenerative chambers (outlet chambers) on the other side and releases heat to the regenerators. Finally, it flows sequentially down to the gas distribution room, the tee pipe, and the outlet. The purge air flows into the gas distribution room through the tee pipe. The VOCs remaining in the purge chamber are blown into the oxidation chamber and mixed with the intake in the oxidation chamber.

Table 1 shows the states of the regenerative chamber in a cycle. The regenerators switched a period counterclockwise by

Table 1. Corresponding Statuses of the Regenerative Chamber for CRTO in a Cycle

time (s)	period number	inlet chamber (intake period)	dead zone chamber (dead period)	outlet chamber (exhaust period)	purge chamber (purge period)
0−30	(1)	01−05	06	07−11	12
30−60	(2)	02−06	07	08−12	01
60−90	(3)	03−07	08	09−12.01	02
.....					
150−180	(6)	06−10	11	12.01−04	05
.....					
240−270	(9)	09−12,01	02	03−07	08
.....					
330−360	(12)	12,01−04	05	06−10	11

the valves every 30 s (Figure 2 and Table 1). It can be seen that each regenerative chamber underwent a sequential period consisting of intake, purge, exhaust, and dead zone. The inlet and outlet regenerative chambers were symmetrical; the regenerative chambers of the purge and no-airflow dead zone separated the inlet and the outlet chambers.

2.2. Physical Model. Figure 3 shows the physical model. Diameters of the regenerative chamber and oxidation chamber were both 3250 mm. The center of the regenerative chamber was a central column without a gas flow. The height of the regenerative chamber was 1000 mm, and that of the oxidation chamber was 2560 mm.

2.3. Simulation Hypothesis and Settings. The simulation hypothesis boundary conditions were set as follows:

(1) VOCs were set as methanol, toluene, and ethyl acetate. The gas was uniform mixed and set as ideal incompressible fluid, the same as Hao.[26]
(2) The outer wall of the CRTO had a 300 mm-thick insulation layer in industry. Therefore, the simulation set the outer wall as an insulation wall.
(3) The heat release of the VOCs could achieve a stable operation of CRTO in industry. Therefore, burner combustion was not considered in the simulation.
(4) The gas could fully exchange heat with the regenerator in the regenerative chamber.

The boundary conditions were set as follows:

(1) The inlet velocity and flux at 343 K in its entrance were 3.30 m/s and 10,000 m^3/h, respectively.
(2) The purge velocity and flux at 293 K in its entrance were 9.35 m/s and 1000 m^3/h, respectively.
(3) The exhaust outlet was set as a pressure outlet. The hydraulic diameter was 1.28 m.
(4) The mass fractions of methanol, toluene, and ethyl acetate were 1.59×10^{-3}, 1.20×10^{-3}, and 1.19×10^{-3}, respectively.
(5) The regenerator was made by the ceramic shaped with plate. Its density was 2.35 g/cm^3. The specific heat capacity was 1250 J/(kg·K). The thermal conductivity was 2.5 W/(m·K), and the porosity was 62.6%.

https://doi.org/10.1021/acsomega.3c08352
ACS Omega 2024, 9, 15893−15903

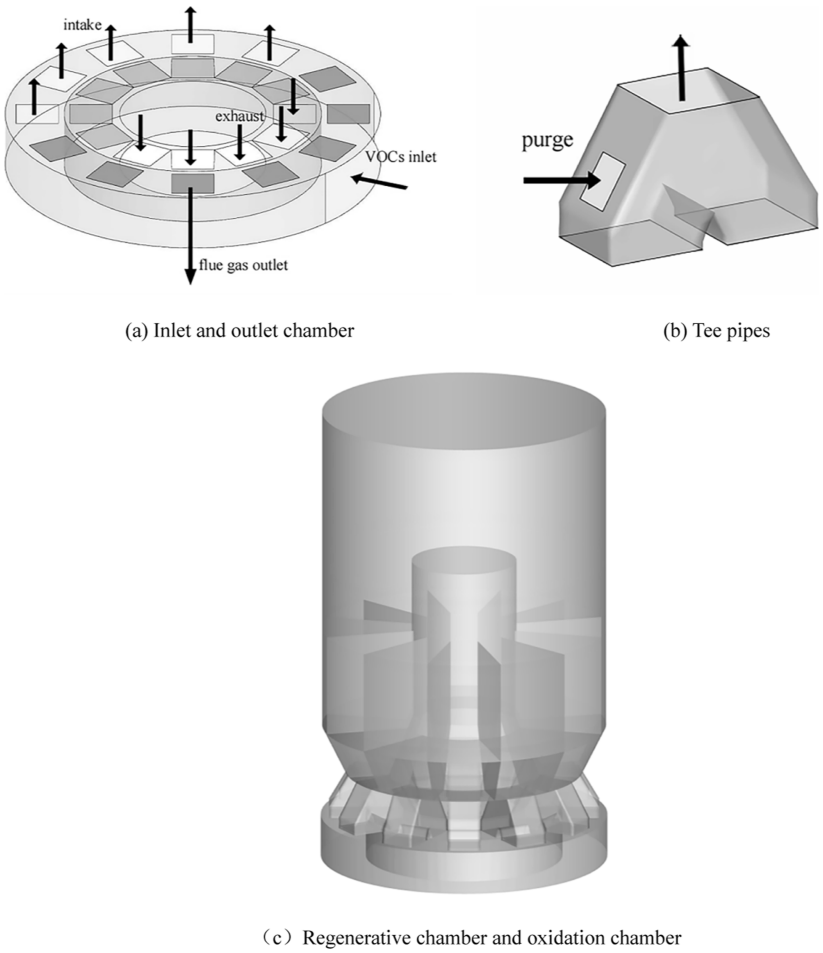

(a) Inlet and outlet chamber (b) Tee pipes

(c) Regenerative chamber and oxidation chamber

Figure 3. CRTO physical model.

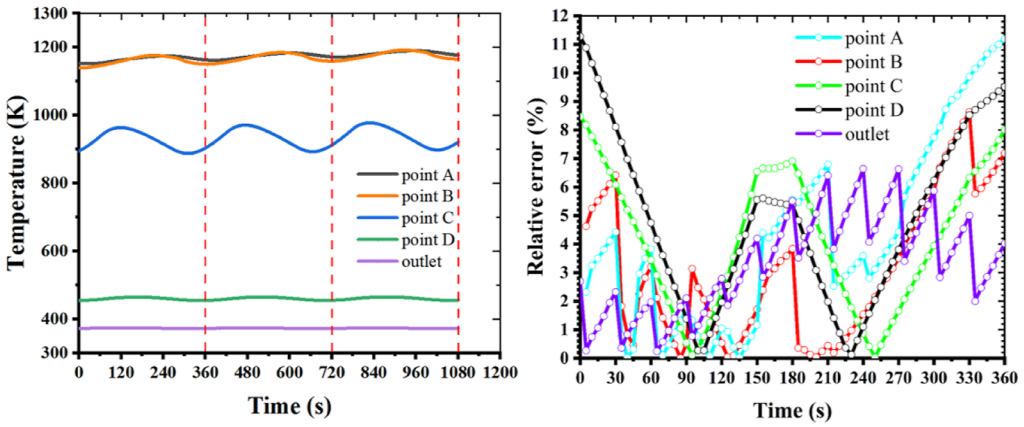

(a) Experimental temperature (b) Temperature error

Figure 4. Experimental temperature (a) and error between experiment and simulation (b).

The standard k−ε model was set as the turbulence model.[11,34]

The finite-rate model considers the elementary reactions of the combustion process, and the chemical reaction rate in the model is a function of the temperature and activation energy. The finite-rate model uses the Arrhenius formula to represent the chemical reaction rate.[37,38] The finite-rate model and the eddy dissipation model are combined into the finite-rate/eddy dissipation model. In the model, the generation or consumption rate of each component is taken as the minimum value of the Arrhenius reaction rate and the eddy dissipation rate. The reaction of air and VOCs in RTO releases a large amount of heat. So the Finite-Rate/Eddy-Dissipation model was adopted.

Scattering and refraction parameters of the gas were hard to get. The DO (Discrete-Ordinates) radiation model does not consider these parameters, and it is widely used and accurate. So, the DO model was used to control the radiation and the heat transfer of the polar gases such as CO_2 and H_2O.[21,39]

https://doi.org/10.1021/acsomega.3c08352
ACS Omega 2024, 9, 15893−15903

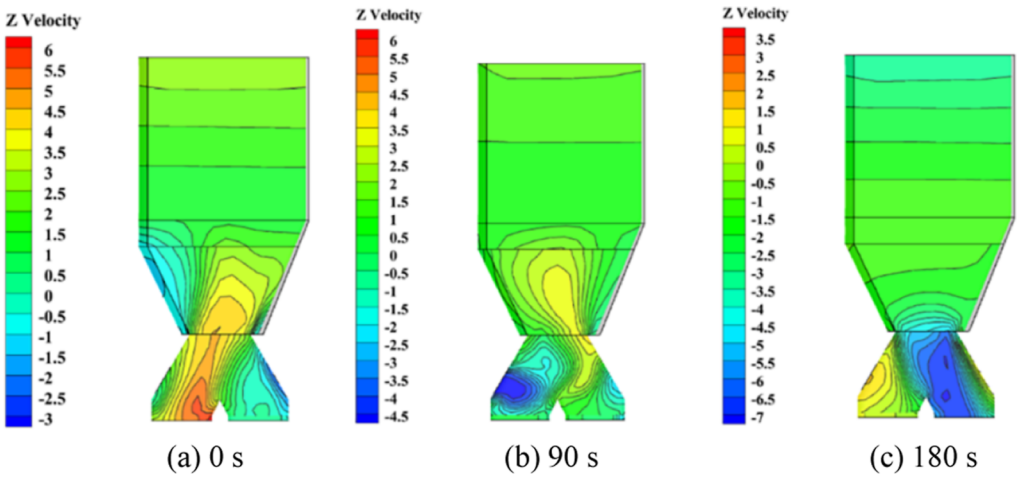

Figure 5. Longitudinal velocity between the NO. 5 tee pipe and regenerative chamber in m/s at (a) 0 s, (b) 90 s, and (c) 180 s.

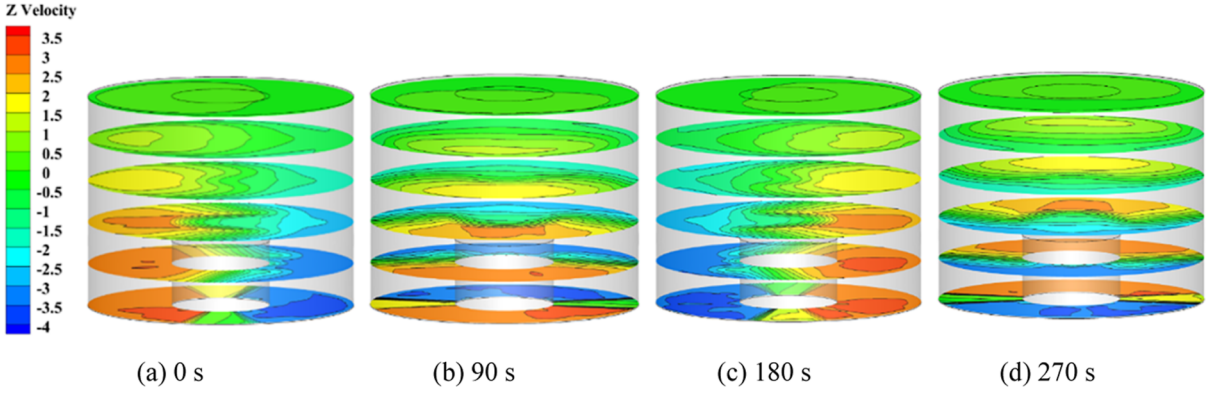

Figure 6. Longitudinal velocity in the oxidation chamber in m/s at (a) 0 s, (b) 90 s, (c) 180 s, and (d) 270 s.

The regenerator was set as a porous medium. In the porous medium model, the viscous and inertial loss terms are important components of the momentum source term,[11,40] which is simple and expressed by

$$S_i = -\left(\frac{\mu}{\alpha}v_i + \frac{1}{2}\rho|v|v_i\right) \quad (1)$$

where μ is the kinematic viscosity of the flow, α is the permeability, v is the velocity vector, C_2 is the inertial resistance coefficient, and ρ is the fluid density of the flow. The solution for the viscous and inertial resistance coefficients are typically available using the semiempirical Ergun equation, which is expressed by

$$\frac{1}{\alpha} = \frac{150}{D_p^2}\frac{(1-\varepsilon)^2}{\varepsilon^3} \quad (2)$$

$$C_2 = \frac{3.5}{D_p}\frac{1-\varepsilon}{\varepsilon^3} \quad (3)$$

where D_p is the mean pore size and ε is the porosity.

The maximum number of the calculation iterations was 20 in time step of each 1 s during the transient simulation.

2.4. Model Verification. Figure 4 shows the experimental temperature and temperature error between the experiment and simulation. Points A−D correspond to the thermocouples in Figure 1. The experimental data were collected every 5 s with no fuel added in three cycles. The temperature distribution had obvious periodicity. The maximum error was 11%, and the minimum one was close to 0. Therefore, this simulation method can be used for the subsequent research.

3. SIMULATION RESULTS

3.1. Longitudinal Velocity in CRTO. *3.1.1. Longitudinal Velocity between Tee Pipe and Regenerative Chamber.* The regenerative chamber of 05 in Figure 2 was selected. 0, 90, and 180 s in Figure 5 corresponded to the intake, purge, and exhaust periods, respectively. There was no gas flow in 270 s, which corresponded to the dead period. Thus, no analysis was made in 270 s. Since the transverse velocity was much lower than the longitudinal velocity, the longitudinal (Z-axis in Figure 1) velocity was selected for analysis.

Figure 5 shows the longitudinal velocity between the tee pipe and the regenerative chamber of 05. After entering the tee pipe from the bottom, the inlet gas in the intake period rushed upward into the gas distribution room, resulting in a nonuniform flow (Figure 5a). However, the porous structure of the regenerator made the flow uniform rapidly after entering the regenerative chamber.[34] Purge flowed in from the left of the tee pipe with a low flow rate (Figure 5b). The velocity stratification of the outlet gas in the exhaust period in the regenerative chamber was obvious (Figure 5c). The gas flow caused a strong vortex in the tee pipe, resulting in fairly large pressure losses.

3.1.2. Longitudinal Velocity in Oxidation Chamber. Figure 6 shows the longitudinal velocity in the oxidation chamber. It

https://doi.org/10.1021/acsomega.3c08352
ACS Omega 2024, 9, 15893−15903

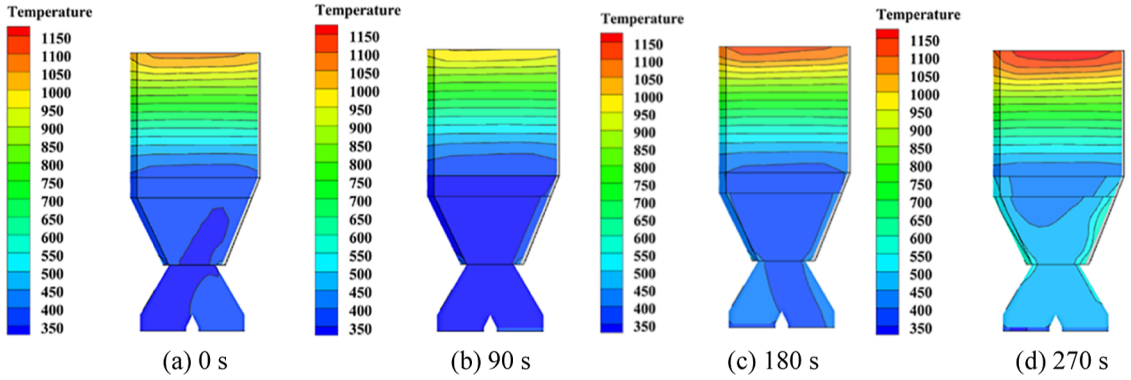

Figure 7. Gas temperature between the NO. 5 tee pipe and regenerative chamber in K at (a) 0 s, (b) 90 s, (c) 180 s, and (d) 270 s.

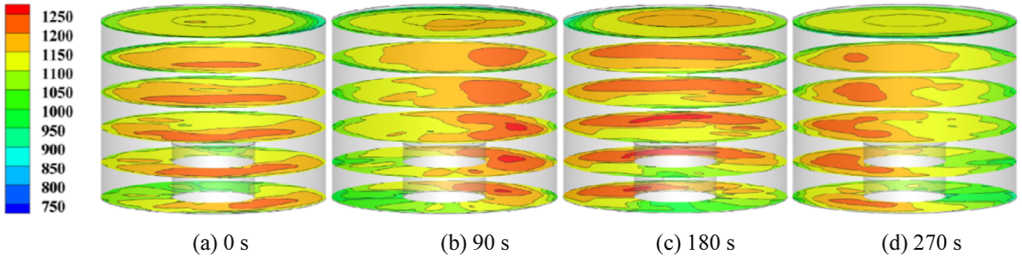

Figure 8. Temperature in the oxidation chamber in K at (a) 0 s, (b) 90 s, (c) 180 s, and (d) 270 s.

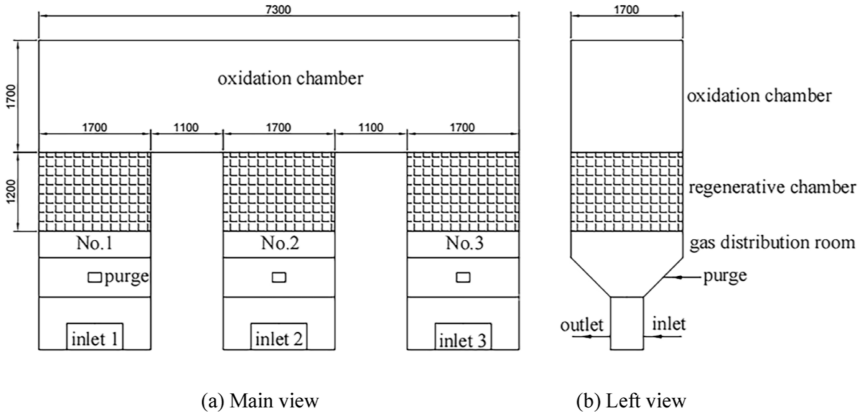

Figure 9. Structure of the TRTO.

can be seen that the velocity gradient was relatively obvious. The velocity distribution of the oxidation chamber showed the same regulation at each period, but this regulation rotated along the cylindrical axis as the periods switched. Therefore, the velocity and residence time distribution of the gas in the oxidation chamber were the same for different periods. However, both the velocity distribution and residence time varied greatly in different periods of TRTO.[26]

3.2. Temperature in CRTO. *3.2.1. Temperature between Tee Pipe and Regenerative Chamber.* Figure 7 shows the gas temperature between the tee pipe and the regenerative chamber of 05. It can be seen that temperature stratification in the regenerative chamber was obvious. Both the inlet gas in Figure 7a and the purge air in Figure 7b from the left of the tee pipe absorbed heat from the regenerator. Thus, the temperature of the regenerator kept dropping during the intake and purge periods. The high-temperature gas from the oxidation chamber continued to heat the regenerator in the exhaust period (Figure 7c). Thus, the temperature of the regenerator in the exhaust period increased. During the dead period, the temperature within the regenerator reached the highest (Figure 7d). There was no heat exchange between the tee pipe and the gas distribution room below the regenerator, so their temperature difference was small.

In industrial applications, the purge air to the regenerative chamber (set as the dead zone) was shut down for a while. It was found that the purging air had little effect on the temperature and the heat exchange in the regenerative chamber. The VOCs in the regenerator could be removed to the oxidation chamber in a short time (less than 1/4 of the period time). Therefore, the time of the purge period can be shorter than that of the intake or exhaust periods in order to reduce the regenerator heat loss by the purge. However, it is not recommended to reduce the purge flux.

3.2.2. Temperature Distribution of Oxidation Chamber. Figure 8 shows the temperature in the oxidation chamber. Temperature of the rising flow from the inlet and the dead zone chambers was low in the oxidation chamber. The

https://doi.org/10.1021/acsomega.3c08352
ACS Omega 2024, 9, 15893−15903

temperature increased as the VOCs oxidized and diffused. But the temperature in the oxidation chamber was not uniform, especially the wall showed the lowest temperature. Similar to the longitudinal velocity distribution, the temperature distribution rotated along the cylinder axis as the periods switched.

4. COMPARISON BETWEEN TRTO AND CRTO

4.1. TRTO Model. TRTO and CRTO, known as the second and third generations of RTO, respectively, are both widely used in China. A TRTO was simulated and compared with the CRTO in order to gain a deeper understanding of RTO. Figure 9 shows the structure of the TRTO. The main parameters of the TRTO [oxidation chamber volume, regenerator volume, and regenerative chamber superficial velocity (0.93 m/s)] were the same as those of the CRTO. However, the CRTO regenerator had a height of 1200 mm, which was 200 mm higher than that of the TRTO at the same regenerator volume and superficial velocity. With reference to the industrial applications, the structure below the TRTO regenerative chamber mainly included intake inlet and exhaust outlet, purge inlet, and gas distribution room.

The cycles of the TRTO and CRTO were both 360 s. Accordingly, the switching time of each period for the TRTO was 120 s. The working states of the three regenerative chambers are listed in Table 2. The simulation method followed that used by Hao.[26]

Table 2. Corresponding States of the Regenerative Chamber for TRTO in a Cycle[2]

time (s)	period number	inlet chamber (intake period)	outlet chamber (exhaust period)	purge chamber (purge period)
0–120	(1)	no. 1	no. 2	no. 3
120–240	(2)	no. 2	no. 3	no. 1
240–360	(3)	no. 3	no. 1	no. 2

4.2. Velocity Comparison in the Regenerative Chamber. Figure 10 shows the regenerator surfaces in comparison. The bottom of the regenerator was selected as the reference surface. Surfaces were selected at an interval of 10% height from the bottom to the top in Figure 10.

Figure 11 shows the average velocity of the regenerative chamber surfaces. Four faces were selected at every 20% height from the regenerator bottom to its top. The distance between each surface and the regenerator bottom can be seen in Figure 11. Height of the TRTO regenerator was 200 mm higher than that of the CRTO. The intake or exhaust volume of the regenerative chamber from CRTO was 5/6 (Table 1) of the total volume, while that of TRTO was 2/3 (Table 2). So, the CRTO regenerator has a larger area for intake and exhaust than that in TRTO. The velocity in the CRTO regenerator was low compared to that in TRTO and had little fluctuation at the same gas flux. The velocity in the regenerator changed stepwise because the CRTO switched the regenerative chambers every 30 s.

4.3. Temperature Comparison in the Regenerative Chamber. Figure 12 shows the average gas temperature of the regenerator surfaces. The regenerator released heat to gas, and the regenerator temperature continued to decrease during the intake period. The regulation was reversed during the exhaust period.

The time of the intake and exhaust periods of a CRTO regenerative chamber was 150 s, which was longer than the 120 s of the TRTO. The regenerator volume of heat storage used by CRTO for heat exchange increased by 1/6 compared to that by TRTO at the same total regenerator volume. The CRTO provided more efficient heat exchange than that of the TRTO.

4.4. Uniformity of the Velocity and the Temperature in the Regenerative Chamber. The coefficient of variation (CV) was used to calculate the uniformity of the regenerative chamber during the intake and exhaust periods, which is expressed by

$$\mathrm{CV} = \frac{\sigma}{|\mu|} \tag{4}$$

where σ represents the standard deviation and μ represents the average.

The calculation results are listed in Figure 13. The velocity and temperature were nonuniform in the lower and top parts of the regenerative chamber due to the inlet or the outlet effects. TRTO had stronger velocity and temperature fluctuations than those in CRTO. Low fluctuation, which indicates high uniformity, is more advantageous for heat transfer.

The CV of each height was averaged, and the results are shown in Table 3. The regenerator volume of the CRTO in intake and exhaust periods were larger than those of the TRTO. Accordingly, the velocity and temperature distribution of the CRTO were more uniform than those of the TRTO.

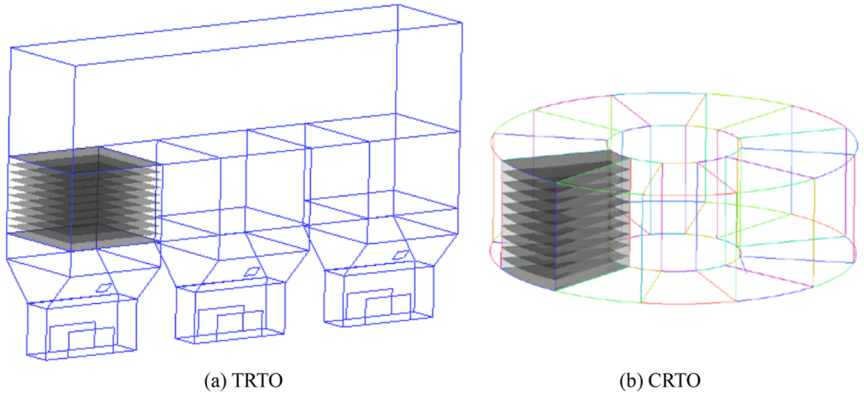

Figure 10. Selected regenerator surfaces in the regenerative chamber for (a) TRTO and (b) CRTO.

https://doi.org/10.1021/acsomega.3c08352
ACS Omega 2024, 9, 15893−15903

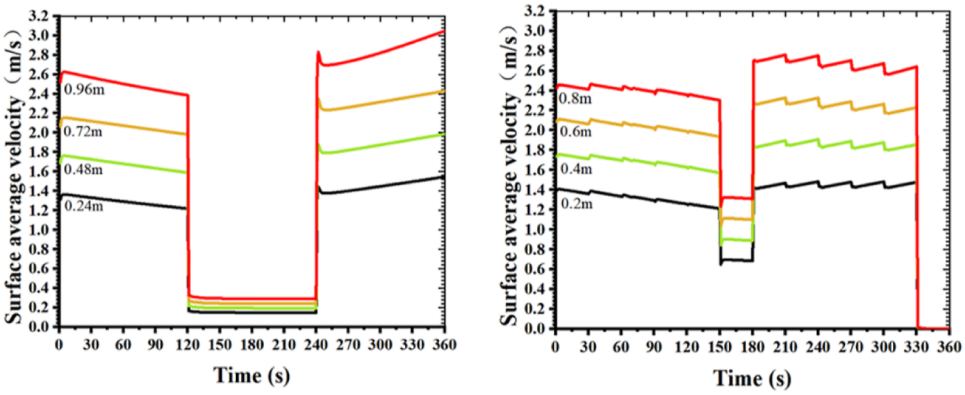

(a) TRTO (b) CRTO

Figure 11. Average velocity of the regenerator surfaces for (a) TRTO and (b) CRTO.

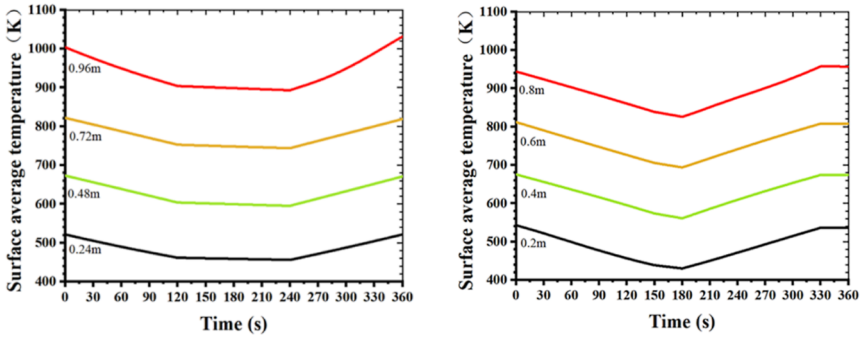

(a) TRTO (b) CRTO

Figure 12. Average gas temperature of the regenerator surfaces in (a) TRTO and (b) CRTO.

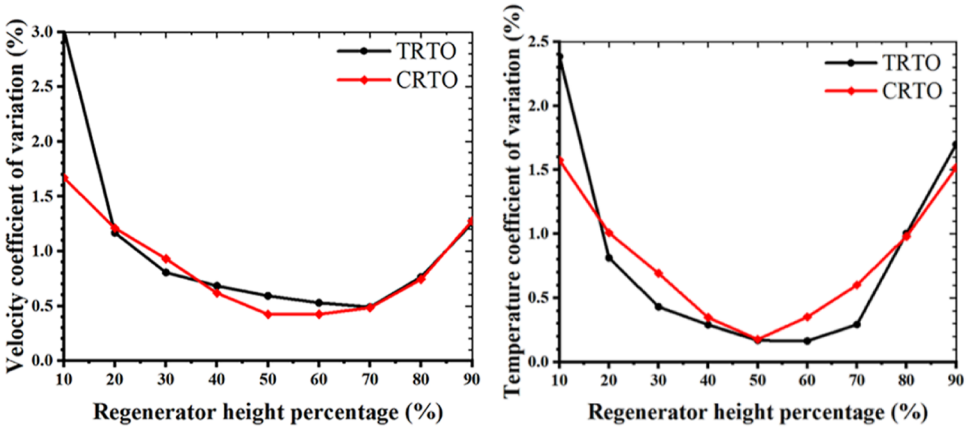

(a) Velocity CV (b) Temperature CV

Figure 13. CV at (a) velocity CV and (b) temperature CV in the intake period.

Table 3. Average CV of the Regenerative Chamber

period		intake	exhaust
TRTO	velocity (%)	1.03	1.21
	temperature (%)	0.81	1.17
CRTO	velocity (%)	0.86	1.05
	temperature (%)	0.81	1.08

Moreover, the intake period with a lower gas temperature was more uniform than the exhaust period.

4.5. Comparison of the Thermal Efficiency. The calculation method for thermal efficiency is shown in eq 5

$$\eta = \frac{Q_{out}(T - T_{out})}{Q_{in}(T - T_{in}) + Q_{purge}(T - T_{purge})} \times 100\% \quad (5)$$

where Q_{in} is inlet gas flux (m^3/h); T_{in} is average temperature of the inlet gas (K); Q_{out} is outlet gas flux (m^3/h); T_{out} is average temperature of the outlet gas (K); Q_{purge} is purge air flux (m^3/h); T_{purge} is average temperature of the purge air (K); and T is average temperature of the oxidation chamber (K).

Figure 14 shows the thermal efficiency with time of TRTO and CRTO in a cycle. The midpoints of each period were connected by the red line. The thermal efficiency was mainly

https://doi.org/10.1021/acsomega.3c08352
ACS Omega 2024, 9, 15893−15903

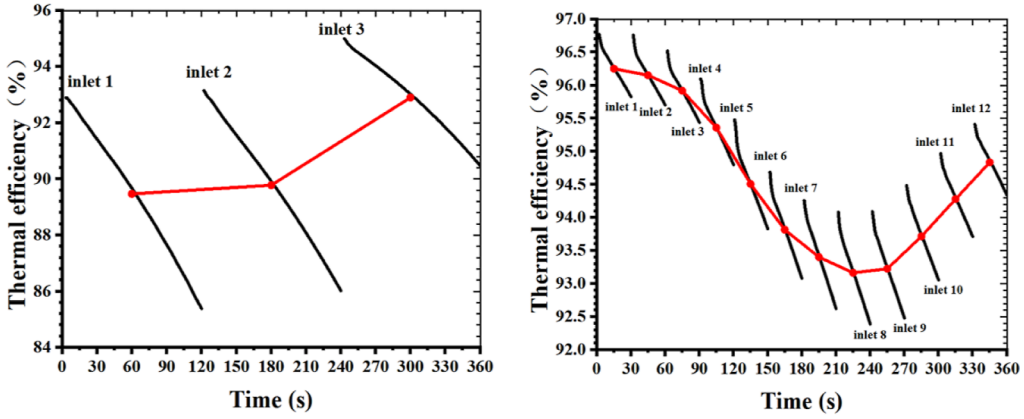

(a) TRTO (b) CRTO

Figure 14. Thermal efficiency with time of (a) TRTO and (b) CRTO in a cycle.

affected by the oxidation chamber temperature and outlet temperature when the inlet temperature remained constant. The thermal efficiency at the beginning of the next period was higher than that at the end of the previous period because the switched regenerative chambers had already absorbed or released heat.

During the intake and exhaust periods, the temperature of the oxidation chamber decreased due to the gradual decrease in the heat released by the regenerator to the gas. High-temperature gas flowed from the oxidation chamber to the regenerative chamber. However, due to the limited heat storage capacity of the regenerator, the heat in the regenerator gradually became saturated during the exhaust period, which increased the RTO outlet temperature. Therefore, the thermal efficiency kept decreasing at every period (Figure 14).

CRTO had more regenerators in heat exchange during the intake or exhaust periods. Therefore, CRTO utilized heat storage more fully than the TRTO. It can be seen from Figure 14 that the average thermal efficiency of CRTO in a cycle was calculated to be 94.55%, which was greater than TRTO's 90.72%.

The temperature in the oxidation chamber of TRTO was more nonuniform, and the time of its period was four times that of CRTO, so its thermal efficiency fluctuates greatly. The thermal efficiency of the curve inlet 3 shown in Figure 14a was the highest. The reason was that the gas had the longest residence time in the oxidation chamber when no. 3 and no. 1 regenerative chambers were in the inlet and outlet chambers (Table 2 and Figure 9), respectively. The average thermal efficiency of each period in Figure 14b fluctuated mainly due to the periodic changes in the oxidization chamber and outlet temperatures.

In addition, adopting the height of the regenerative chamber to analyze the thermal efficiency is more insightful. The height was also the main indicator in previous studies. However, it is recommended to use the regenerator volume to analyze the thermal efficiency when the volumes are different.

5. CONCLUSIONS

The velocity and temperature of a CRTO with 12 regenerative chambers during a cycle or a period are studied for the first time. The CRTO is compared to a TRTO with the same main parameters. The main conclusions are as follows:

(1) Longitudinal velocity and temperature of the CRTO from the tee pipe to the regenerative chamber bottom are nonuniform, and the inertia of the airflow causes significant vortices, which increase the apparatus resistance. The velocity and temperature became uniform rapidly with obvious stratification after flowing into the regenerative chamber.

(2) Longitudinal velocity and temperature gradient in the CRTO oxidation chamber are obvious. However, the distribution in the oxidation chamber is not related to CRTO's inlet and outlet positions or the structure under the regenerative chamber after homogenization by the regenerator unit. That is, the velocity and temperature distribution of the oxidation chamber show the same regulation at each period, but this regulation rotates along the cylindrical axis as the period switched.

(3) The CRTO regenerator has a larger area for intake and exhaust than that in TRTO. So, the velocity and temperature fluctuations in the CRTO regenerative chamber are smaller and more uniform than those in TRTO, with a coefficient of variation increase of approximately 2%.

(4) The time of the intake and exhaust periods of a CRTO regenerative chamber are both 150 s, which is 30 s longer than those of the TRTO. The intake or exhaust volume of the regenerative chamber from CRTO is 5/6 of the total volume, while that of TRTO is 2/3. The average thermal efficiency of CRTO is about 3% higher than that of TRTO. Comprehensively speaking, CRTO had a better effect.

In future work, research will be conducted on the elemental reactions of VOCs in regenerator, combustion, and flame theory within regenerative and oxidation chambers.

AUTHOR INFORMATION

Corresponding Author

Xiaowen Hao − *Harbin Institute of Technology, Weihai, Shandong 264209, China*; Email: haoxiaowen@yeah.net

Authors

Kaiming Ren − *Harbin Institute of Technology, Weihai, Shandong 264209, China*

Zhijun Zhang − *China Construction Eighth Engineering Group First Construction Co., Ltd., Jinan, Shandong 250000, China*

https://doi.org/10.1021/acsomega.3c08352
ACS Omega 2024, 9, 15893−15903

Haixiang Qin − *Harbin Institute of Technology, Weihai, Shandong 264209, China*
Jianyu Tan − *Harbin Institute of Technology, Weihai, Shandong 264209, China*

Complete contact information is available at: https://pubs.acs.org/10.1021/acsomega.3c08352

Funding

This research is supported by Key R&D Program of Shandong Province, China(grant no. 2022ZLGX04) and Design and preparation of nickel-based microscale porous electrodes and development of small electrolysis water hydrogen production equipment(grant no. 2022KYCXJJ01) provided by the Harbin Institute of Technology, Weihai.

Notes

The authors declare no competing financial interest.

■ ACKNOWLEDGMENTS

Funding from Key R&D Program of Shandong Province, China and Design and preparation of nickel-based microscale porous electrodes and development of small electrolysis water hydrogen production equipment is gratefully acknowledged. Thanks to Associate Professor Hao for his careful guidance and Professor Tan for his advice on model design. Thanks to Zhang and Qin for valuable discussions and timely help.

■ REFERENCES

(1) Lewandowski, D. A. *Design of Thermal Oxidation Systems for Volatile Organic Compounds*; CRC Press 2017..
(2) Han, S. B.; Hua, Y. Y.; Lin, Y. S.; Yao, L. C.; Wang, Z. C.; Zheng, Z. J.; Yang, J.; Zhao, C. H.; Zheng, C. H.; Gao, X. Fault diagnosis of regenerative thermal oxidizer system via dynamic uncertain causality graph integrated with early anomaly detection. *Process Saf. Environ. Prot.* **2023**, *179*, 724−734.
(3) Marín, P.; Díez, F. V.; Ordóñez, S. Reverse flow reactors as sustainable devices for performing exothermic reactions: applications and engineering aspects. *Chem. Eng. Process.* **2019**, *135*, 175−189.
(4) Gosiewski, K.; Pawlaczyk, A.; Jaschik, M. Thermal combustion of lean methane-air mixtures: flow reversal research and demonstration reactor model and its validation. *Chem. Eng. J.* **2012**, *207*−*208*, 76−84.
(5) Choi, B. S.; Yi, J. Simulation and optimization on the regenerative thermal oxidation of volatile organic compounds. *Chem. Eng. J.* **2000**, *76* (2), 103−114.
(6) Gao, P. F.; Gou, X. L. Experimental research on the thermal oxidation of ventilation air methane in a thermal reverse flow reactor. *ACS Omega* **2019**, *4* (12), 14886−14894.
(7) Kuang, R.; Liu, Y. Y.; An, T. Z.; Shen, Y. J. Numerical analysis of oxidation performance of basalt fiber bundle thermal flow-reversal reactor. *Appl. Therm. Eng.* **2022**, *215*, 118886.
(8) Panwar, K.; Murthy, D. S. Analysis of thermal characteristics of the ball packed thermal regenerator. *Procedia Eng.* **2015**, *127*, 1118−1125.
(9) Marín, P.; Díez, F. V.; Ordóñez, S. A new method for controlling the ignition state of a regenerative combustor using a heat storage device. *Appl. Energy* **2014**, *116*, 322−332.
(10) Granadero, D.; Garcia-Muñoz, A.; Adam, R.; Omil, F.; Feijoo, G. Evaluation of abatement options to reduce formaldehyde emissions in vehicle assembly paint shops using the Life Cycle methodology. *Clean. Environ. Syst.* **2023**, *11*, 100139.
(11) Sun, B.; Zhao, T.; Li, L.; Wang, Z. L.; Sun, P.; Peng, C. Optimization of regenerator operating parameters and thermal insulation construction for rotary regenerative thermal oxidizer (r-RTO) based on thermal-fluid coupling method and quadratic regression model. *Case Stud. Therm. Eng.* **2022**, *37*, 102314.
(12) Wang, X. X.; Zhou, F. B.; Ling, Y. H.; Xiao, Y. N.; Ma, B.; Ma, X. Z.; Yu, S. B.; Liu, H.; Wei, K. W.; Kang, J. H. Overview and outlook on utilization technologies of low-concentration coal mine methane. *Energy Fuels* **2021**, *35* (19), 15398−15423.
(13) Amelio, M.; Morrone, P. Numerical evaluation of the energetic performances of structured and random packed beds in regenerative thermal oxidizers. *Appl. Therm. Eng.* **2007**, *27* (4), 762−770.
(14) You, Y. H.; Huang, H.; Shao, G. W.; Hu, J.; Xu, X. C.; Luo, X. B. A three-dimensional numerical model of unsteady flow and heat transfer in ceramic honeycomb regenerator. *Appl. Therm. Eng.* **2016**, *108*, 1243−1250.
(15) Shi, Y. Y.; Liu, Y. Q.; Zhou, Y. Q.; Sun, P.; Mao, M. M.; Zhang, Y. Q. Study on dynamic heat extraction characteristics of heat exchanger tube embedded in thermal flow reverse reactor for heat recovery. *Process Saf. Environ. Prot.* **2022**, *162*, 846−858.
(16) Noh, D. S.; Hong, S. K.; Ryou, H. S.; Lee, S. H. An experimental and numerical study on thermal performance of a regenerator system with ceramic honeycomb. *J. Mech. Sci. Technol.* **2001**, *15* (3), 357−365.
(17) Chou, M. S.; Hei, C. M.; Huang, Y. W. Regenerative thermal oxidation of airborne N, N-dimethylformamide and its associated nitrogen oxides formation characteristics. *J. Air Waste Manag.* **2007**, *57* (8), 991−999.
(18) You, Y. H.; Wu, Z. D.; Li, B.; Zhang, Z.; Pan, S. T.; Xu, X. C. 3D numerical simulation and optimization of honeycomb regenerators with parallel or crosswise arrangement of circular holes. *Chem. Eng. Process.* **2019**, *137*, 22−27.
(19) Giuntini, L.; Bertei, A.; Tortorelli, S.; Percivale, M.; Paoletti, E.; Nicolella, C.; Galletti, C. Coupled CFD and 1-D dynamic modeling for the analysis of industrial regenerative thermal oxidizers. *Chem. Eng. Process.* **2020**, *157*, 108117.
(20) Zhou, Y. Q.; Shi, Y. Y.; Liu, Y. Q.; Sun, P.; Mao, M. M. Experimental and simulation research on heat extraction characteristics from a pilot-scale reverse flow reactor for low-grade energy. *Appl. Therm. Eng.* **2023**, *220*, 119761.
(21) Wang, F. Z.; Lei, X.; Hao, X. W. Key factors in the volatile organic compounds treatment by regenerative thermal oxidizer. *J. Air Waste Manag.* **2020**, *70* (5), 557−567.
(22) Liu, F. L.; Ren, K. M.; Pei, J. Y.; Zhao, X. Z.; Hao, X. W. Heat transfer characteristics in regenerator cell for gaseous organic compound treatment. *J. Mech. Sci. Technol.* **2023**, *37* (2), 1001−1010.
(23) Wang, Y. X.; Zhu, T. The efficiency of Pd addition and Sr substitution on $La_{1-x}Sr_xMnO_3$ to remove ventilation air methane in a catalytic flow reversal reactor. *Atmosphere* **2022**, *13* (1), 54.
(24) Lan, B.; Li, Y. R.; Zhao, X. S.; Kang, J. D. Industrial-scale experimental study on the thermal oxidation of ventilation air methane and the heat recovery in a multibed thermal flowreversal reactor. *Energies* **2018**, *11* (6), 1578.
(25) Gosiewski, K.; Pawlaczyk-Kurek, A. Aerodynamic CFD simulations of experimental and industrial thermal flow reversal reactors. *Chem. Eng. J.* **2019**, *373*, 1367−1379.
(26) Hao, X. W.; Li, R. X.; Wang, J.; Yang, X. F. Numerical simulation of a regenerative thermal oxidizer for volatile organic compounds treatment. *J. Korean Soc. Environ.* **2018**, *23* (4), 397−405.
(27) Gosiewski, K.; Pawlaczyk-Kurek, A. Impact of thermal asymmetry on efficiency of the heat recovery and ways of restoring symmetry in the flow reversal reactors. *Int. J. Chem. React. Eng.* **2019**, *17* (3), 20180021.
(28) Pu, G.; Li, X.; Yuan, F. Numerical study on heat transfer efficiency of regenerative thermal oxidizers with three canisters. *Processes* **2021**, *9* (9), 1621.
(29) Lan, B.; Li, Y. R. Numerical simulation of thermodynamic performance in a honeycomb ceramic channel. In *Proceedings of the 3rd International Symposium on Mine Safety Science and Engineering, 3rd International Symposium on Mine Safety Science and Engineering (ISMS)*, 2016; pp 219−224.
(30) Zhang, G. Y.; Li, Q. Z.; Liu, X. X.; Lin, B. Q.; Li, D. M. Investigations on the mitigation of ventilation air methane and energy

recovery in site trial thermal flow-reversal reactor. *Chem. Eng. Process.* **2022**, *170*, 108703.
(31) Heidari-Kaydan, A.; Hajidavalloo, E. Three-dimensional simulation of rotary air preheater in steam power plant. *Appl. Therm. Eng.* **2014**, *73* (1), 399−407.
(32) Zhang, X.; Yuan, J.; Tian, Z.; Wang, J. Estimation of the direct leakage of rotary air preheaters based on temperature distribution modeling. *Int. J. Heat Mass Transf.* **2019**, *134*, 119−130.
(33) Wang, L.; Li, D.; Zhu, H.; Chen, G.; Luo, H.; Che, D. Investigation on regenerative heat exchanger with novel low-leakage system for flue gas denitration in steel industry. *Appl. Therm. Eng.* **2020**, *178*, 115483.
(34) Mao, M. M.; Gao, M.; Shi, J. R.; Liu, Y. Q.; Sun, S.; Li, J. Experimental and numerical study of flame stability in a rotary flow reversal reactor with ultra-lean toluene/air mixture. *Chem. Eng. Process.* **2023**, *192*, 109484.
(35) Waste Gas Purification Committee of CAEPI. *Development report on organic waste gas control industry in 2016*; China Environmental Protection Industry, 2017; Vol. *11*, pp 5−16.
(36) *Emission standard of air pollutants for printing industry; DB11/1201*; Beijing, China, 2023.
(37) Yao, Z. X.; Saveliev, A. V. High Efficiency High Temperature Heat Extraction from Porous Media Reciprocal Flow Burner: Time-averaged Model. *Appl. Therm. Eng.* **2018**, *143*, 614−620.
(38) Li, W.; Klemeš, J. J.; Wang, Q. W.; Zeng, M. Numerical analysis on the improved thermo-chemical behaviour of hierarchical energy materials as a cascaded thermal accumulator. *Energy* **2021**, *232*, 120937.
(39) Li, J.; Mao, M. M.; Gao, M.; Chen, Q.; Shi, J. R.; Liu, Y. Q. A Multi-scale numerical model for investigation of flame dynamics in a thermal flow reversal reactor. *Energies* **2022**, *15* (1), 318.
(40) Alhadhrami, A.; Vishalakshi, C. S.; Prasanna, B. M.; Sreenivasa, B. R.; Alzahrani, H. A.; Punith Gowda, R. J.; Naveen Kumar, R. Numerical simulation of local thermal non-equilibrium effects on the flow and heat transfer of non-Newtonian Casson fluid in a porous media. *Case Stud. Therm. Eng.* **2021**, *28*, 101483.

https://doi.org/10.1021/acsomega.3c08352
ACS Omega 2024, 9, 15893−15903